Chapter 7

Rigorous Approach to Analysis of Two-Dimensional Potential Problems, Wave Propagation and Scattering for Multi-conductor Systems

Galyna Safonova and Elena Vinogradova

Additional information is available at the end of the chapter

http://dx.doi.org/10.5772/61287

Abstract

The research described in this chapter analyses two-dimensional potential problems for the multi-body systems, transverse electromagnetic wave propagation along multi-conductor transmission lines and two-dimensional plane wave scattering by various arrays. All conductors may be of arbitrary cross-sections; the only restriction on the system geometry is a smooth parameterization. These problems are mathematically modelled by Dirichlet boundary value problems for either the Laplace or the Helmholtz equation, with the classical integral representation of the solutions in the form of single-layer potential. The analytical-numerical algorithm presented here is based on the method of analytical regularization. The key idea behind this technique is an analytical transformation of the initial ill-posed integral equations to a well-conditioned Fredholm second kind matrix equation. The resulting system of infinite linear algebraic equations is effectively solved using the truncation method: the solution of the truncated system converges to the solution of the infinite system with the guaranteed accuracy that only depends on the truncation number and thus may be pre-specified. The solution obtained is applied to the accurate analysis of 2-D electrostatic- and electrodynamic-field problems for multi-conductor systems with arbitrary profiled conductors. Examples of some conceptual shielded transmission lines incorporating various configurations of conductors and scattering problems for the arrays of thick strips establish the utility of our method and its reliability in various situations

Keywords: Scattering, propagation, analytical regularization, Laplace equation, Helmholtz equation

1. Introduction

In electrostatic and electromagnetic studies of highly elongated cylinders, and ensembles or arrays of such cylinders, it is well-known [1] that the most important effects can be treated by replacing the three-dimensional structure by the corresponding cross-sectional two-dimensional (2D) profile. Such cylinders are described by $a << L$, where L is the length of the cylinder, and a is a parameter characterizing its cross-section. This condition ensures that for real objects such as charged conducting cylinders, the field induced by their ends will have no impact on electric field distribution well away from the ends, or this impact will be vanishingly small as $L \to \infty$. Such idealization in 2D electrostatics causes nonphysical solutions: the arbitrary profiled charged cylinder, for instance, generates a potential that logarithmically grows instead of vanishing as expected at distant observation points. This means that the potential is unbounded at infinity. The nonphysical nature of the solution is commented by many authors. However, for systems of charged conductors this difficulty can be avoided in one of two ways: by setting the net charge of the system to be equal to zero or by introducing earthed infinite planes or closed earthed shields. This issue is discussed in [2]. In spite of the seeming limitations that the above conditions enforce on 2D electrostatic modelling, they naturally occur in almost all problems arising in practice. In particular, 2D boundary value problems for the Laplace and Helmholtz equation describe many problems of practical interest arising aero- and hydrodynamics (potential fluid flow), electrostatics, electromagnetic scattering studies, acoustics, elasticity theory, etc.

The long-standing interest in the investigation of the electrostatic field in periodic structures continues because of numerous applications. One example is the analysis of the propagation of the transverse electromagnetic (TEM) wave in open and shielded multi-conductor transmission lines [3, 4]. When the contour of a conductor coincides with the coordinate surface of one of the coordinate systems in which the Laplace's equation is separable, the Fourier method (method of separation of variables) is used. More generally, a variety of potential problems have been solved by the conformal mapping method. These results are described in many classical handbooks and monographs. The number of such solved problems is highly restricted. Nowadays, the need for simulation of devices used in practice requires development of more universal methods to tackle problems with objects of various finite-width shapes. One of such numerous examples is the capacitance calculation for thick electrodes [5] where a physically reasonable meaning of 'edge capacitance' arises only because an accurate charge distribution over the whole electrode could not be accurately calculated. Though solutions obtained for single objects may adequately describe the real situation, most practical problems deal with a finite number of objects (say, conductors). Even when a conductor is of canonical shape (circular or elliptic cylinder), the solution of an electrostatic multi-conductor problem for an assembly of cylinders of different radii is a very bulky and lengthy procedure. Solving this problem as a classical boundary value problem for Laplace's equation and enforcing the pre-assigned boundary conditions at the surface of each conductor, it is necessary to make multiple re-expansions of the eigen functions of the Laplace's equation in each local coordinate system in terms of that chosen to satisfy the boundary conditions.

http://dx.doi.org/10.5772/61287

Electromagnetic and acoustic problems described by the Helmholtz equation can also be considered in two dimensions. A great variety of publications consider the problem involving infinite gratings. They are often used in antenna applications as polarizers and filters. In [6], a vector diffraction formulation for the analysis of perfectly conducting gratings of finite width and thickness is presented. The grating is assumed to have a finite number of infinitely long arbitrarily shaped rods, and is illuminated by an arbitrary plane wave. Electric and magnetic field integral equations are used to numerically solve the corresponding TM and TE electromagnetic problems. Periodic structures in the millimetre wave range are considered in [7]: this paper studies single and double periodic devices using a semi-analytical mode-matching technique. Diffraction of the TM-polarized Gaussian beam by N equally spaced slits (finite grating in a planar perfectly conducting thick screen) is investigated in [8]. Numerous publications consider the different types of arrays. A general approach was presented in [9] for solving the 2D scattering of a plane wave by an arbitrary configuration of perfectly conducting circular cylinders in front of a plane surface with general reflection properties. Acoustic scattering by a cluster of small sound-soft obstacles was considered in [10]. The 2D scattering of a Gaussian beam by a periodic array of circular cylinders is studied in [11]. A study of the electromagnetic scattering from multi-layered periodic arrays of parallel circular cylinders is presented in [12]. The electromagnetic scattering by multiple perfectly conducting arbitrary polygonal cylinders is analysed in [13].

It should be noted that the long history of solving the Laplace and Helmholtz equations is marked by the development of many numerical methods which are useful in simulation of practical devices. Such methods include the finite difference technique, extrapolation [14], point-matching method [15], boundary element method [16], spectral-space domain method [17], finite element method [18-20], transverse modal analysis [21] and mode-matching method [22]. A numerical integral equation approach is used in [23] to explore plane-wave scattering from a nonplanar surface with a sinusoidal height profile for the case of the magnetic field parallel to the surface ridges (TM polarization). In spite of effectiveness of these methods in many cases and flexibility in geometrical representation of the structures, modelling of ridges still have some substantial drawbacks. Most of the methods require large resources in terms of computational time and storage. Often the solutions obtained with such purely numerical methods need to be verified through comparison to other results: accuracy generally cannot be guaranteed for a greater number of iterations or larger-scale computations. This problem becomes pronounced in some topologically complex configurations. In electromagnetics, the corresponding class of numerical solutions is applicable in the low to intermediate frequency range. Resonant systems behaviour cannot be reliably analysed with the numerical techniques (see [24]). Analytical-numerical methods such as those based on the method of analytical regularization (MAR) are designed to overcome these drawbacks in the resonant regime. A comparative analysis of the MAR and other methods was conducted in [25], and in [26] the distinctive features of each of the discussed methods are clearly described. The above-mentioned methods are mostly suited for analysis of a single or very few conductors. In the case of a significant number of conductors with individual profiles, the effectiveness of such purely numerical methods is highly problematic because of the rapidly growing scale of computations.

In order to address these difficulties, we present here a semi-analytical approach to the analysis of 2D electrostatic and electrodynamic field problems for multi-conductor systems. The problems to be solved are treated as the classical Dirichlet boundary value problems for the Laplace and Helmholtz equations. It is well-known [27, 28] that solutions to the Laplace and Helmholtz equations can be represented as a single-layer potential at points exterior to the body of a single conductor with contour S is given by

$$U(q) = \int_S G(p,q)Z(p)dS_p \tag{1}$$

where $Z(p)$ is related to the linear charge distribution on the contour S in the case of the Laplace equation, and to the linear current density in case of the Helmholtz equation. $G(p, q) = -\frac{1}{2\pi}\log|p-q|$ is the Green's function for Laplace's equation in 2D space. If the contour S is charged to some prescribed potential value V_0, then $Z(p)$ may be found by solving the equation:

$$-\frac{1}{2\pi}\int_s \log|p-q|Z(p)dS_p = V_0, \qquad q \in S_p \tag{2}$$

This equation may be classified as a first kind Fredholm equation with a singular kernel; it is ill-posed [29]. Nevertheless, this problem has been tackled by many authors who used direct numerical schemes for solving its discrete analogue in a form of a first kind algebraic equation. Theoretically, any numerical method applied to solve this equation is unable to guarantee uniform convergence, or pre-determined computational accuracy.

The only way to avoid these shortcomings is to transform the initial equation into a second kind Fredholm equation, discretization of which guarantees uniform convergence and any pre-determined accuracy of the numerical solution depending on truncation number. We employ the MAR, in particular, described in [30, 31]. An accurate solution to wave scattering by a single infinitely long cylinder of arbitrary cross-section by the MAR was obtained in [32]. The details of the algorithm for cylinders of closed arbitrary profile are presented in [26, 31]. In this chapter, we generalize the MAR for a multi-conductor potential problem where each body is an arbitrary profiled cylinder.

2. Regularization of the electrostatic problem: MAR

2.1. Problem statement

Consider (N-1) arbitrary profiled charged perfect electric conductor (PEC) cylinders embedded into a homogeneous dielectric medium with relative permittivity ε_r (Figure 1). The finite dielectric medium is bounded by the infinitesimally thin, grounded cylindrical shell.

http://dx.doi.org/10.5772/61287

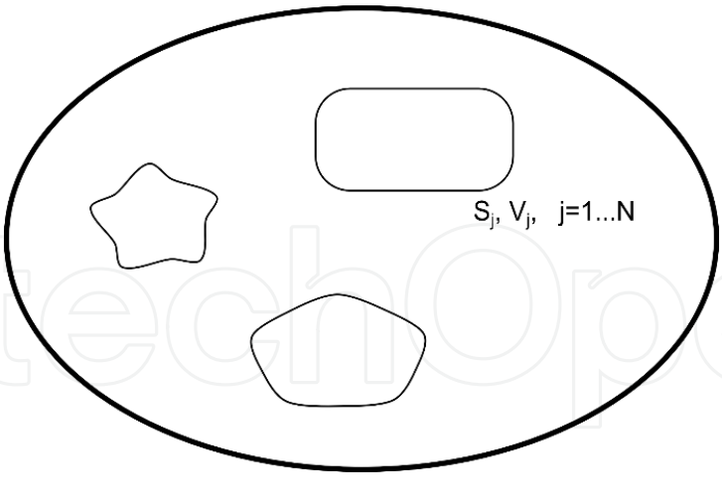

Figure 1. Problem geometry.

The problem is to find electrostatic potential U elsewhere inside the shielded region. This electrostatic problem is fully described by the Dirichlet boundary value problem for the Laplace equation:

$$\Delta U = 0 \tag{3}$$

with boundary conditions of the potentials V_n given at the surface of each of N cylinders:

$$U\big|_{S_n} = V_n, n = 1,...,N-1;\ U\big|_{S_N} = V_N = 0. \tag{4}$$

To employ the regularization procedure, all contours S_n must be smooth enough and non-self crossing to provide their continuous parameterization and twice differentiation at each point of S_n.

2.2. Problem solution

The main challenge of this problem is that all the conductors are arbitrary-shaped and the classical separation of variables method is not applicable here. We use a more general approach based on an integral representation. Using the superposition principle, we seek the solution for the total field potential U as the sum of the single-layer potentials contributed by each cylinder:

$$U(q) = \sum_{j=1}^{N} \int_{S_j} G(|p-q|) Z_j(p) dS_p; \tag{5}$$

where Z_j is the unknown line charge density of the j th conductor scaled by $4\pi/\varepsilon$, S_j is the boundary contour of the j th conductor and points q lie in the area between the contours. The Kernel G of the integral equation (5) is the 2D free space Green's function:

$$G = -\frac{1}{2\pi}\log\left(|p-q|\right) \tag{6}$$

where $|p-q|$ is the distance between points q and p.

Applying boundary conditions to (5), one can arrive at the coupled system of integral equations for the unknowns Z_j :

$$-\sum_{j=1}^{N}\int_{S_j} G_{ij}\left(|p-q|\right)Z_j(p)dl_p = V_n,\ i=1,...,N \tag{7}$$

Equation (7) represents a system of first kind Fredholm integral equations that is generally ill-posed.

The contours of the conductors' cross-sections should be smooth. Thus for the analysis of the rectangular and square conductors, corners should be smoothed. The two most common types of parameterization are by angle and by arc length. Here, we use parameterization by angle. After parameterization of the contours $\eta(\theta)\equiv(x(\theta),\ y(\theta))$ and introducing some new notations:

$$\begin{aligned} &z_j = l_j(\theta)Z_j\left(\eta_j(\theta)\right),\ \ l(\theta) = \left\{\left[x'(\theta)\right]^2 + \left[y'(\theta)\right]^2\right\}^{1/2}, \\ &R_{sj}(\theta,\tau) = |p-q| = \left|\eta_s(\theta)-\eta_j(\tau)\right| = \left\{\left[x_s(\theta)-x_j(\tau)\right]^2 + \left[y_s(\theta)-y_j(\tau)\right]^2\right\}^{1/2}, \end{aligned} \tag{8}$$

we obtain the system of N integral equations:

$$-\sum_{j=1}^{N}\int_{-\pi}^{\pi} G\left(R_{sj}(\theta,\tau)\right)z_j(\tau)d\tau = V_s(\theta),\ s=1,2...N. \tag{9}$$

The described approach permits us to consider a broader set of possible boundary conditions than simply a constant, though in the application to be described, a constant is deployed on the RHS of (9).

For the kernels $G(R_{sj}(\theta,\ \tau))$ such that $s\neq j$, points corresponding to θ and τ belong to different contours and so $R_{sj}(\theta,\ \tau)\neq 0$ everywhere; hence, the corresponding integral terms do not contain singularities. For $G_{ss}(\theta,\ \tau)$ the corresponding integral contains a singularity of loga-

http://dx.doi.org/10.5772/61287

rithmic type at the points $\theta=\tau$. In this case, we analytically separate the Green's function into the singular part and a remainder L^{sj} that does not contain any singularity:

$$\begin{aligned} -2\pi G\left(R_{sj}(\theta,\tau)\right) &= \log\left(R_{sj}(\theta,\tau)\right) = L^{sj}(\theta,\tau), \quad s \neq j, \\ -2\pi G\left(R_{sj}(\theta,\tau)\right) &= \log\left(R_{sj}(\theta,\tau)\right) = L^{sj}(\theta,\tau) + \log\left(2\sin\left|\frac{\theta-\tau}{2}\right|\right), \quad s = j. \end{aligned} \tag{10}$$

Now we can determine L^{sj} from (10) as follows:

$$\begin{aligned} L^{sj}(\theta,\tau) &= \log\left(R_{sj}(\theta,\tau)\right) - \log\left(2\sin\left|\frac{\theta-\tau}{2}\right|\right), \quad s = j; \\ L^{sj}(\theta,\tau) &= \log\left(R_{sj}(\theta,\tau)\right), \quad s \neq j. \end{aligned} \tag{11}$$

The function L^{sj}, $s=j$ is a regular function, defined everywhere except at points $\theta=\tau$; the function L^{sj}, $s\neq j$ is defined everywhere. It can be shown that for the Laplace's equation this regular function has the same degree of smoothness as the contour parameterization. An exact expression for L^{sj}, $s=j$ at the points of singularity where $\theta=\tau$ was obtained analytically:

$$L^{sj}(\theta,\tau) = \log\left(l(\theta)\right), \tag{12}$$

where $l(\theta)=\sqrt{x(\theta)^2 + y(\theta)^2}$ is an arc length in the point θ.

Now we can redefine function L^{sj}, $s=j$ everywhere by the formula:

$$L^{sj} = \begin{cases} \log(R_{sj}(\theta,\tau)) - \log\left(2\sin\left|\frac{\theta-\tau}{2}\right|\right), \theta \neq \tau, \\ \log\left(l(\theta)\right), \theta = \tau. \end{cases} \tag{13}$$

Using the well-known Fourier expansion, we can formulate an expression for the singular part of the Green's function:

$$\log\left(2\sin\left|\frac{\theta-\tau}{2}\right|\right) = \frac{1}{2}\sum_{\substack{n=-\infty \\ n\neq 0}}^{\infty} \frac{e^{in(\theta-\tau)}}{|n|}, \tag{14}$$

As the function L^{sj} is regular, we can expand it into double Fourier series:

$$L^{sj}(\theta,\tau)=\sum_{n=-\infty}^{\infty}\sum_{m=-\infty}^{\infty} l_{nm}^{sj}\, e^{i(n\theta+m\tau)}. \tag{15}$$

Also the unknown function z_j and the given potential function are represented by their Fourier series:

$$z_j(\tau)=\sum_{-\infty}^{\infty}\xi_n^j e^{in\tau}, \qquad V_j(\theta)=\sum_{-\infty}^{\infty}v_n^j e^{in\theta} \tag{16}$$

After substitution of all expansions into (9), one can arrive at the system of N integral equations:

$$\sum_{n=-\infty}^{\infty}\frac{\xi_n^s}{|n|}e^{sn\theta}-2\sum_{j=1}^{N}\sum_{n=-\infty}^{\infty}e^{in\theta}\left(\sum_{m=-\infty}^{\infty}l_{n,-m}^{sj}\xi_m^j\right)=\sum_{n=-\infty}^{\infty}v_n^j e^{sn\theta},\ \theta\in[-\pi,\pi],\ \ s=1,2,...,N. \tag{17}$$

Using orthogonal properties and completeness of the functions $\{e^{in\varphi}\}_{n=-\infty}^{n=\infty}$ and defining the rescaled unknown Fourier coefficients of charge density function ξ_n^s as follows: $\tilde{\xi}_n^s=\frac{\xi_n^s}{\sigma_n}$, $\sigma_n=|n|^{1/2}$ when $n\neq 0$ and $\sigma_0=1$, we obtain the following infinite system of linear algebraic equations:

$$\tilde{\xi}_n^s(1-\delta_{n0})+\sum_{j=1}^{N}\sum_{m=-\infty}^{\infty}\sigma_n\sigma_m l_{n,-m}^{sj}\tilde{\xi}_m^j=\sigma_n v_n^s,\ n=0,\pm1,\pm2...;\ s=1,2,...,N. \tag{18}$$

Following the steps suggested in [33], it can be shown that coefficient matrix in (18) is square summable:

$$\sum_{j=1}^{N}\sum_{m=-\infty}^{\infty}|\sigma_n\sigma_m l_{n,-m}^{sj}|^2<\infty,\ n=0,\pm1,\pm2...;\ s=1,2,...,N. \tag{19}$$

Thus the infinite system (18) is of a second Fredholm kind and can now be effectively solved by a truncation method. The solution of the truncated system monotonically and rapidly converges to the exact solution. The above solution automatically incorporates the reciprocal influence of all charged cylinders, allowing accurate calculation of the line charge densities on the boundaries and then the field potentials at any point of the space between the conductors. Fourier expansions in (18) are calculated numerically as all functions are regular.

http://dx.doi.org/10.5772/61287

3. Regularization of the Dirichlet problem for Helmholtz equation: MAR technique for the *N*-body multiple scattering

3.1. Statement of the problem

In this section, we consider the scattering problem for the structure which consists of N arbitrary profiled perfect electric -conductor cylinders embedded into a homogeneous dielectric medium with relative permittivity ε. The main steps of the solution algorithm are similar to those which were carried out to obtain the solution to the Laplace equation, presented in Section 2.2.

The scattered electromagnetic field U^s obeys the Helmholtz equation:

$$\left(\Delta + k^2\right)U^s\left(p\right) = 0, \tag{20}$$

where point p lies exterior to the structure S, $k=2\pi/\lambda$ is the wave number and λ is the corresponding wave length.

Here we consider incident fields in the form of a plane wave. We focus on a transverse magnetic (TM) wave polarization of the incident field (U^0), therefore the scattered field should satisfy the Dirichlet boundary condition on metallic surfaces:

$$U^s(p) = -U^0(p), \qquad p \in S. \tag{21}$$

The field should also satisfy the Sommerfeld radiation condition:

$$U^s\left(p\right) = O\left(\left|p\right|^{-1/2}\right); \frac{\partial U^s(p)}{\partial\left|p\right|} - ikU^s\left(p\right) = O\left(\left|p\right|^{-1/2}\right), \tag{22}$$

As $|p|\to\infty$ where $|p|$ is the radial component of the point p in the arbitrary fixed polar coordinate system.

3.2. Regularized solution

Solutions to the Laplace equation can be represented as a single-layer potential at points exterior to the body. Using the superposition principle, we seek the solution as the sum of single-layer potentials contributed by each cylinder:

$$U\left(q\right) = \sum_{n=1}^{N} \int_{L_n} G\left(\left|p_n - q\right|\right) Z_n\left(p_n\right) dl_{p_n}. \tag{23}$$

Here $G(|p_n-q|)$ is the relevant free space Green's function depending on the distance $|p_n-q|$ between the observation point q and point p_n lying on the contour S_n: $G(|p-q|)=-\frac{i}{4}H_0^{(1)}(k|p-q|)$, and the function $Z(p)$ is related to the linear current density $J(p)$ as $J(p)=ikcZ/4\pi$ (where k is a wave number, c the light speed).

Applying boundary conditions to (23), we obtain the system of N integral equations:

$$\sum_{j=1}^{N}\int_{L_n} G\left(\left|p_n-q\right|\right)Z_n\left(p_n\right)dl_{p_n}=-U_m^0\left(q\right),\quad q\in S_m, m=1,...,N. \tag{24}$$

After parameterization of the contours $\eta_n(\theta)=(x_n(\theta), y_n(\theta))$ where $\theta\in[-\pi, \pi]$, we use the definition of a line integral and obtain a functional equation in the form:

$$\sum_{j=1}^{N}\int_{-\pi}^{\pi} G\left(R_{mn}\left(\theta,\tau\right)\right)z_n\left(\tau\right)d\tau=-U^0\left(\theta\right). \tag{25}$$

The following notation is used in (25): $z_n(\tau)=l_n(\tau)Z_n(p_n(\tau))$, where $l_n=\sqrt{(x_n(\tau)')^2+(y_n(\tau)')^2}$, $n=1, ..., N$; $R_{mn}(\theta, \tau)$ is the distance between points $\eta_m(\theta)$ and $\eta_n(\tau)$ lying on the m-th and n-th contours, respectively.

The kernel of the integral equation (25) contains a singularity only in the terms $G(R_{mn}(\theta, \tau))$. It is of logarithmic type at the points $\theta=\tau$, and we analytically split the Green's function into a singular and a regular part $H^{mn}(\theta, \tau)$ similarly to the solution steps for the Laplace equation in Section 2.2:

$$G\left(R_{mn}\left(\theta,\tau\right)\right)=-\frac{i}{4}H_0^{(1)}\left(kR_{mn}\left(\theta,\tau\right)\right)=\begin{cases}\dfrac{1}{2\pi}\left(\log\left(2\sin\left|\dfrac{\theta-\tau}{2}\right|\right)+H^{mm}\left(\theta,\tau\right)\right), & m=n\\ \dfrac{1}{2\pi}H^{mn}\left(\theta,\tau\right), & m\neq n,\end{cases} \tag{26}$$

so that the regular part of Green's function is

$$H^{mn}\left(\theta,\tau\right)=\begin{cases}-\dfrac{i\pi}{2}H_0^{(1)}\left(kR_{mm}\right)-\log\left(2\sin\left|\dfrac{\theta-\tau}{2}\right|\right), & m=n\\ -\dfrac{i\pi}{2}H_0^{(1)}\left(kR_{mm}\right), & m\neq n,\end{cases} \tag{27}$$

http://dx.doi.org/10.5772/61287

The function H^{mn}, $m=n$ is a regular function, defined everywhere except at the points $\theta=\tau$; the function H^{mn}, $m\neq n$ is regular everywhere. An exact expression for H^{mm} at the points of singularity is obtained analytically:

$$H^{mm}(\theta,\tau)_{|\theta=\tau} = -\frac{i\pi}{2} + \gamma + \log\frac{k\cdot l_m(\theta)}{2}, \tag{28}$$

where γ is Euler's constant.

We expand the singular part of Green's functions in the same way as in Section 2.2, and perform the double Fourier series expansion for the regular function H^{mm} : $H^{mn}(\theta,\tau)=\sum_{j,l=-\infty}^{\infty} h_{jl}^{mn} e^{i(j\theta+l\tau)}$.

The unknown function z_j is also represented by its Fourier series: $z_n(\tau)=\sum_{p=-\infty}^{\infty} \xi_p^n e^{ip\tau}$.

After substitution of all expansions into (25), one can arrive at the system of N integral equations. Following the regularization steps for the Laplace equation from Section 2.3, we obtain an infinite system of linear algebraic equations of the second kind:

$$\tilde{\xi}_l^m(1-\delta_{n0}) + \sum_{j=n=1}^{N}\sum_{p=-\infty}^{\infty} \sigma_l\sigma_p h_{l,-p}^{mn}\tilde{\xi}_p^n = \sigma_l g_l^m \qquad l=1,2,...,N;\ n=0,\pm1,\pm2...,\tag{29}$$

where the following notations are used:

$$\begin{aligned} \sigma_p &= \begin{cases} |p|^{1/2} & \text{when } n\neq 0 \\ 1 & \text{when } n=0, \end{cases} \\ \tilde{\xi}_p^n &= \sigma_p^{-1}\xi_p^n, \qquad -2U^0 = \sum_{m=-\infty}^{\infty} g_l^m e^{il\theta}. \end{aligned} \tag{30}$$

The infinite systems (31) can be effectively solved by a truncation method. The solution of the truncated system steadily and rapidly converges to the exact solution [34]. There are no limitations on the number of cylinders with arbitrary smooth cross-sections.

4. Numerical results

The numerical code was validated by comparing obtained results with known analytical solutions for the coaxial line with a centred inner conductor [35] and the coaxial line with a shifted inner conductor [36]. Results obtained coincide for up to 16 decimal places with the published solutions starting with N_{tr}=16 for the centred inner conductor and N_{tr}=128 for the

inner conductor located close to the shield. Our results are also in a good agreement with other semi-analytical and numerical techniques (for example, presented in [37]).

As an illustration of the effectiveness of the obtained solution, we calculate the capacitance matrix for the assembly of arbitrary profiled cylinders located inside the grounded shield. There are no limitations on the number of cylinders with arbitrary smooth cross-sections. The high efficiency of the code is also the result of employment of the discrete Fast Fourier Transform. This makes filling of the matrix very fast routine procedure. For example, the computation time for a problem with the four inner cylinders and truncation number $N_{tr}=256$ does not exceed 4.5 s on a standard PC.

Efficiency of the developed method is also illustrated by the behaviour of the normalized truncation error versus truncation number (see [30]) calculated in the maximum norm sense as:

$$e\left(N_{tr}\right)=\frac{\max_{n\le N_{tr}}\left|x_n^{N_{tr}+1}-x_n^{N_{tr}}\right|}{\max_{n\le N_{tr}}\left|x_n^{N_{tr}+1}\right|}, \tag{31}$$

where $\left|\, x_n^{N_{tr}+1}\,\right|_{n=0}^{N_{tr}}$ and $\left\{x_n^{N_{tr}+1}\right\}_{n=0}^{N_{tr}+1}$ denote the solutions to the systems (19) or (29) truncated to N_{tr} and $N_{tr}+1$ equations, respectively. The results of the calculations of truncation error for the infinite system (18) defining the solution to the Laplace equation are shown in the Figure 2. The considered structure is a circular shield of radius 1 with elliptic conductor with major semi-axis $b_1 = 0.5$ and various values of the minor semi-axis b_2, embedded in the centre of the shield.

Figure 3 shows the condition number behaviour in the same case. The results are quite accurate and stable: for a simple structure like this, the condition number has reached a stable value even for small values of the truncation number.

In these examples, the ellipse is parameterized by the angle as a parameter. Fewer number of points on the sides of a slender ellipse results in decreasing accuracy for smaller b_2. Arc length parameterization is one way to overcome this drawback. Other parameterizations could be even more effective, but they often require some adjustments for each shape.

Various shapes of conductor will be considered in this chapter. For all system configurations here and below, the inner conductors' potentials are set to be 1; the shield is grounded. The profile of each interior conductor is described by the super-ellipse equation (32), where function $\rho(\varphi)$ and its derivative are continuous [38], with

$$\rho(\varphi)=\left[\left|\frac{1}{a}\cos\left(m\frac{\varphi}{4}\right)\right|^{n_2}+\left|\frac{1}{b}\sin\left(m\frac{\varphi}{4}\right)\right|^{n_3}\right]^{-1/n_1}. \tag{32}$$

http://dx.doi.org/10.5772/61287

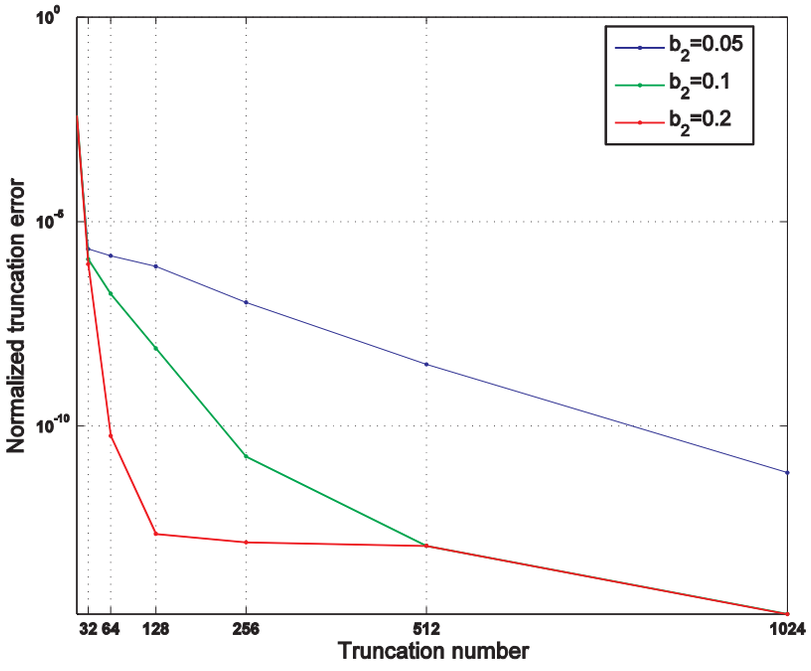

Figure 2. Normalized truncation error versus N_{tr} : major semi-axis of the inner ellipse b_1 = 0.5 and various values of the minor semi-axis b_2.

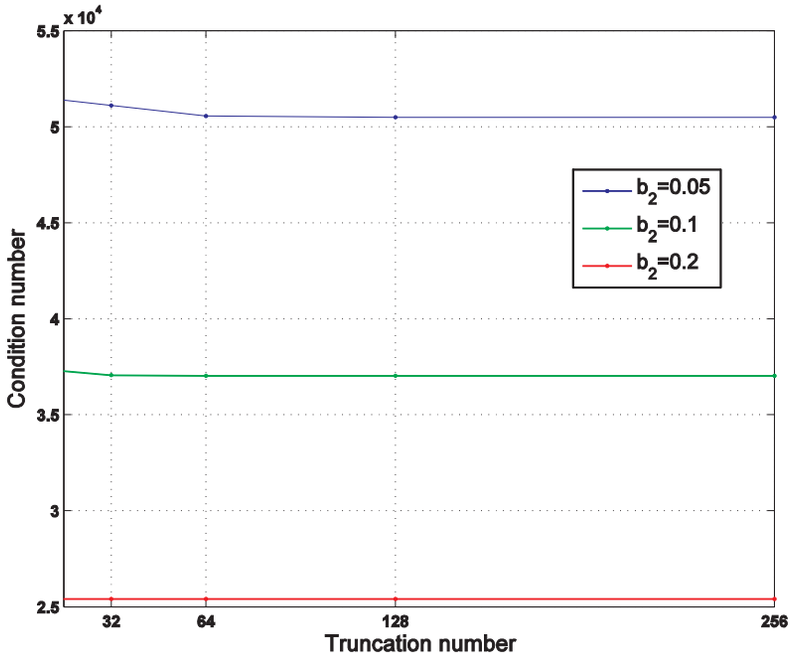

Figure 3. Condition number versus N_{tr}.

In this equation, a and b are the figure size parameters, n_1, n_2, n_3 define corner sharpness and m represents the symmetry. This formula allows us to model a great variety of shapes such as an ellipse ($n=n_1=n_2=n_3=2$, $m=4$), a rectangle with rounded-off corners ($n=n_1=n_2=n_3>2$, $m=4$), a star with the smooth rays ($n_1=2$, $n_2=n_3>2$, m is equal to the number of rays) and many others.

This parameterization is infinitely differentiable which gives us a great advantage in accuracy. To demonstrate this property, comparison of two different parameterizations used in the solution to the Helmholtz equation for a single rectangle with rounded-off corners is presented in Figure 4.

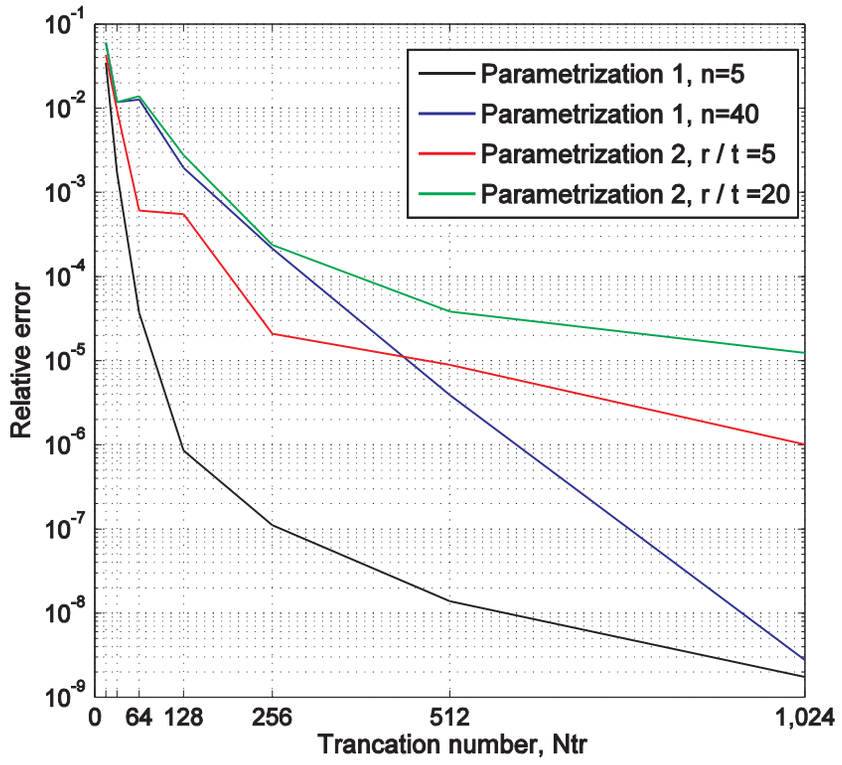

Figure 4. Comparison of super-ellipse and smoothed rectangular parameterizations.

Parameterization 1 stands for a super-ellipse formula; straight lines with a combination of quarter circles are used for the Parameterization 2. The super-ellipse parameterization uses $n=n_1=n_2=n_3$, (see (32)); the greater the n is, the sharper the corners of the rectangle are. Sharper corners require higher truncation number to get the same level of the accuracy due to the parameterization by the angle. In Parameterization 2, r is a radius of curvature used to smoothen the corner, h is rectangle height. In all cases, rectangle height/width ratio is equal to 0.5. Parameterization 2 is not twice differentiable - there is a discontinuity in the second derivative at the joining of the straight line and the quarter circle. This account for slow convergence of the second parameterization as $N_{tr} \to \infty$.

http://dx.doi.org/10.5772/61287

4.1. Electrostatic problems

4.1.1. Multi-conductor transmission lines

Here the power of the method is illustrated by the analysis of multi-conductor transmission lines. Other possible applications of our method for the problems modelled by the Laplace equation include impedance calculations for the transmission lines with adjustable inner conductor, published in [39] and capacitance calculations for the capacitance microscope [40].

The distribution of the electrostatic field for a conceptual configuration of a shielded three-conductor transmission line is shown in Figure 5.

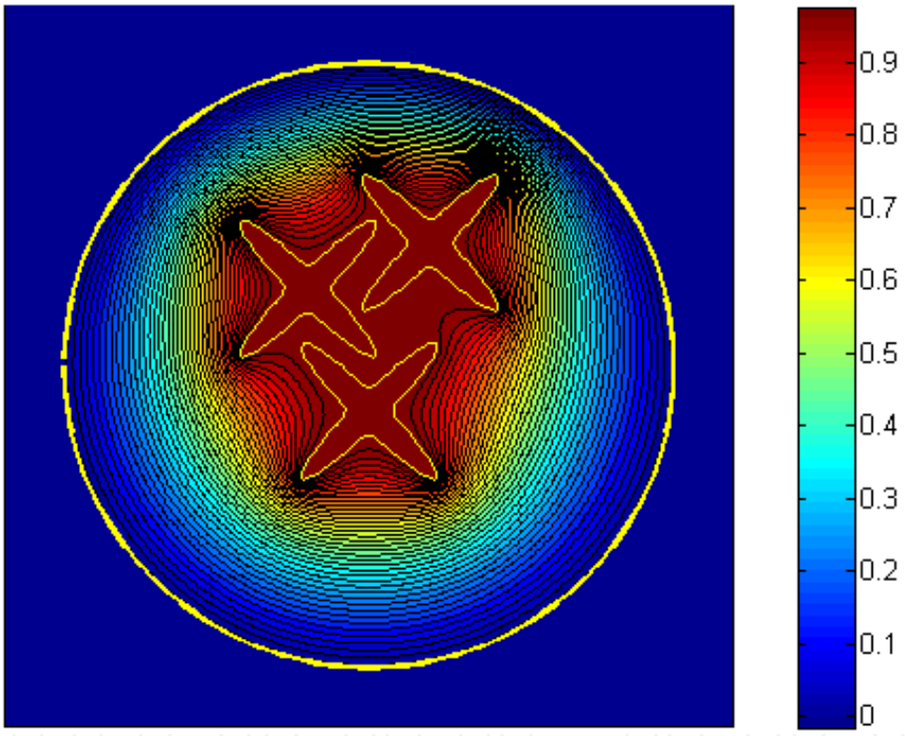

Figure 5. Conceptual circular shielded transmission line with three inner cylinders. ($a=b=0.6$, $m=5$, $n_1=2$, $n_2=n_3=13$).

It is worth noting that apparently sharp edges are in fact not sharp but have a very small radius of curvature at some points due to parameterization of the contours.

Next we present the calculations for the capacitance matrix (Table 1) calculated by formula $C_{i,j}=\partial Q_i/\partial u_j$ in the case of the circular shield and conductors of nearly rectangular cross-section (Figure 4). Here Q_i is a total charge on the i th cylinder, and u_j is the potential of the j th cylinder.

Symmetric alignment:	Non-symmetric alignment:
$C = \begin{pmatrix} 3.5583 & -0.4441 & -0.4441 \\ -0.4441 & 3.5580 & -0.4440 \\ -0.4441 & -0.4440 & 3.5580 \end{pmatrix}$	$C = \begin{pmatrix} 3.5151 & -0.2713 & -0.4191 \\ -0.2713 & 3.8903 & -1.1851 \\ -0.4191 & -1.1851 & 3.9261 \end{pmatrix}$

Table 1. Capacitance matrix values for the structure for the square conductors with a circular shield (see Figure 6).

Two configurations are examined - a symmetrical one and another obtained by the translation of one conductor, as indicated in Figure 6. In each case, accuracy was ensured by examining error estimates as a function of truncation number as explained above.

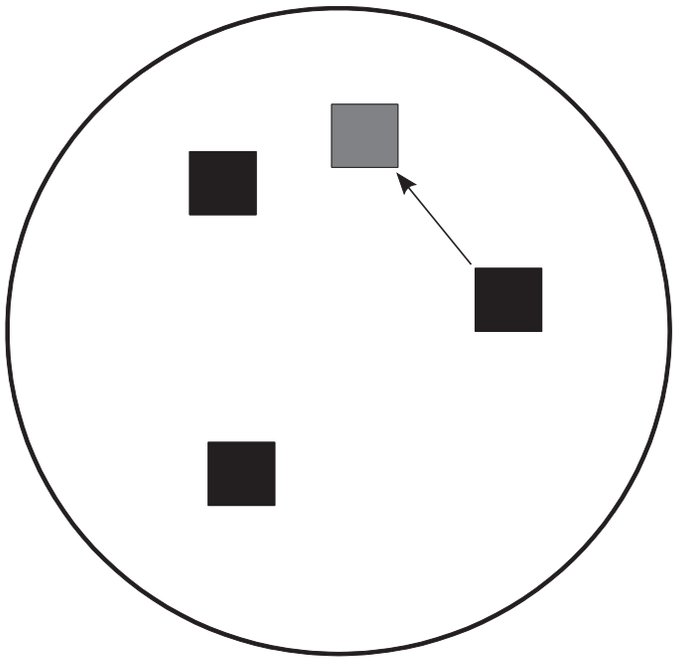

Figure 6. Symmetrical and shifted inner conductors alignment ($a=b=0.1$, $m=4$, $n_1=n_2=n_3=40$).

4.1.2. Transmission lines with the closely spaced conductors

Another example demonstrating the effectiveness of the developed algorithm is a study of the closely spaced conductors case (Figure 7). In Table 2, capacitance values for a circular conductor are shown depending on a distance between the inner conductor of a radius 0.1 and a shield of radius 1. Truncation numbers are chosen to ensure capacitance values and are stable to four decimal places.

The analysis shows that reliable results are obtained when the condition $d \geq \Delta l$ is satisfied, where d is the distance between the conductors, $\Delta l = L / N_{tr}$ is a parameterization step, L is a maximum contour length.

http://dx.doi.org/10.5772/61287

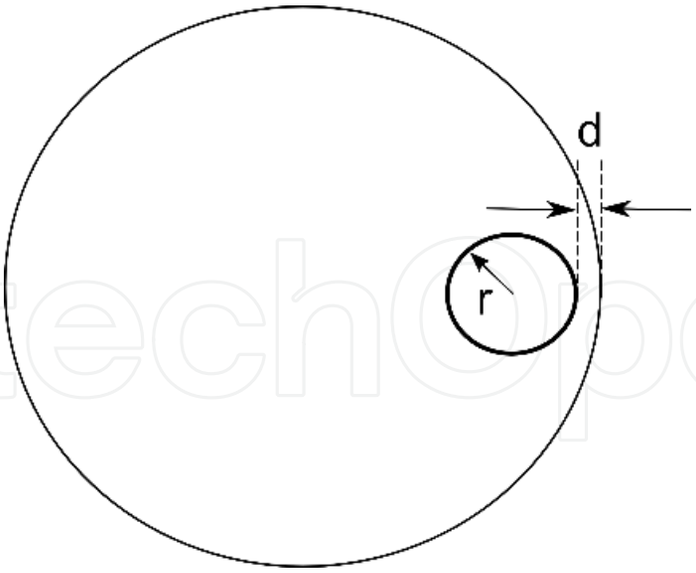

Figure 7. A circular shield with a closely spaced inner conductor.

d/r	N_{tr}	C
1	64	5.1270
0.5	128	6.9491
0.1	512	14.9620
0.05	1024	21.0534

Table 2. Capacitance values for the structure with the closely spaced conductors.

4.2. Scattering of a plane wave by an array of thick strips

Arrays, which are composed of a finite number of strips, are probably the most common periodic structures. They are employed in various electromagnetic radiating and wave-guiding devices. For example, a simple but effective leaky-wave antenna can be designed by placing a microstrip grating above a ground plane, as first proposed by Honey in the 1950s [41] and then studied by different authors with many variations [42]. In addition, periodic structures in the millimetre wave range with high precision requirements must be planar structures, for fabrication reasons [7]. Also, in other applications the strip grating is often used as a circular polarizer [43]. The list of applications can be continued. Nowadays, a lot of attention is paid to more realistic models of the strip gratings: finite gratings, excited by compact directional sources [8]; gratings with thick strips [44, 45]; special elemental positioning [46, 47], etc.

In this section, we consider scattering of an obliquely incident E-polarized plane wave by a finite array of metallic thick strips which is relevant to the problems examined in the papers mentioned above. The case of the array of circular cylinders, including resonant effects, was considered in [48].

4.2.1. Linear array of horizontal thick strips

We consider the scattering of the E-polarized plane wave obliquely incident the linear array composed of the metallic thick strips, as shown in Figure 8. The elemental thick strip is described by its width w and its thickness t. The element spacing is characterized by d. The incidence angle is φ_0. In our calculations, we set $w=1$, so that $k \equiv kw$ is the relative wave number.

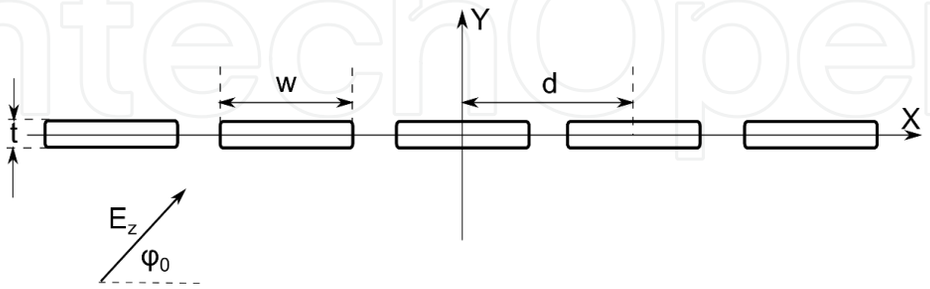

Figure 8. Linear array of horizontal strips.

The radar cross-section (RCS) is determined from the scattered field as $\rho \to \infty$ in the direction $\varphi = \varphi_0 + \pi$, where φ_0 is angle of incidence of the incident plane wave, via

$$RCS = \lim_{\rho \to \infty} 2\pi\rho \left| U^s\left(\rho, \varphi_0 + \pi\right)\right|^2. \tag{33}$$

The dependence of the RCS ($RCS(\varphi_0)$, in dB) on the incidence angle, φ_0, for the 3-, 5- and 9-elements array ($k=\pi$) is shown in Figure 9. As the number of elements grows two peaks occurring away from normal incidence begin to dominate over the other minor maxima, due to specular reflection from the elements of the array. The highest peak corresponds to normal incidence ($\varphi_0 = 90°$); the second peak corresponds to the incidence angle $\varphi_0 = \cos^{-1}(1/1.5) = 48.19°$. The calculation of the current density distribution on the contour of each element is of practical interest, especially for the situations when the results obtained for infinite gratings are used for finite gratings. It is reasonable to assume that the near equal current distribution on all elements of the finite grating is a plausible argument to treat such grating as a fragment of the infinite grating. This idea was used, for example, by Kalhor in [49].

In our calculations, we fix the number of the strips $N=5$ in the grating and calculate the current distribution on each element. The results are shown in Figure 10, where we used the parameters: $\varphi_0 = 90$, $k=\pi$, $t=0.1$, $d=1.5$.

Because of the symmetrical (for normal wave incidence) location of the elements in the array, the distribution $|J_z(\varphi)|$ will be identical for the strips, numerated by the indexes $n = \pm 1$ and $n = \pm 2$. Figure 10 demonstrates that current density distributions on all strips are very close to each other, as a front planar surface of each strip is uniformly illuminated by the incidental plane wave. This induces, in particular, a constant current density on most part of the frontal surface of the strip, except in the narrow region near its corners. The current density $|J_z(\varphi)|$

http://dx.doi.org/10.5772/61287

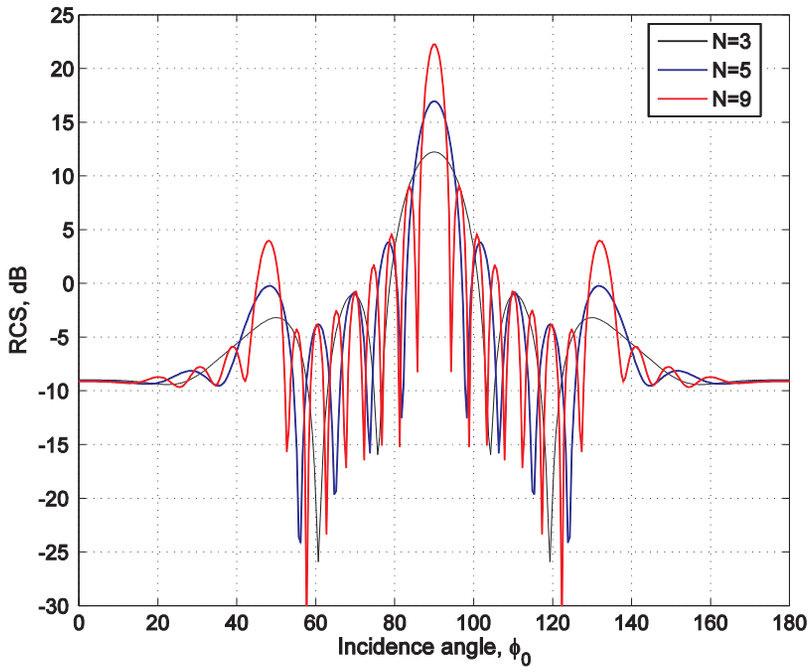

Figure 9. $RCS(\varphi_0),\ (k=\pi,\ t/w=0.1,\ d=1.5)$.

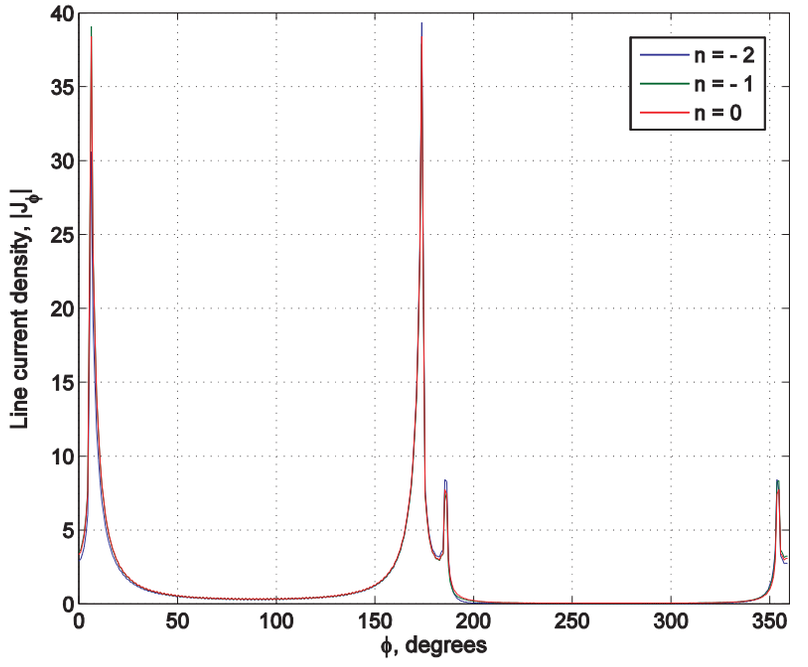

Figure 10. $|J_z(\varphi)|$ at the strips $n=-2,\ 1,\ 0$ in the 5-element array $(k=\pi,\ t/w=0.1,\ d=1.5)$.

has predictable jumps at the angle values, corresponding to the corners of the thick strips. Figure 10 shows four sharp peaks in the distribution of the function $|J_z(\varphi)|$. Two dominant peaks correspond to the directly illuminated corners of the frontal surface of the strip. Two other peaks with significantly smaller magnitude correspond to the corners on the underside of the strip; furthermore, the current density on these parts is relatively small. Due to these peculiarities of the current density distribution on the surface of the thick strip, the dependence of $|J_z(\varphi)|$ on the number of strips in the array is quite weak.

The scattered pattern in the direction φ is defined as

$$SP(\varphi) = \lim_{\rho\to\infty}\left(\left|U^s(\rho,\varphi)\right| / \max_{\varphi\in[-\pi,\pi]}\left|U^s(\rho,\varphi)\right|\right). \tag{34}$$

The distribution of the scattered field in the far-field zone is shown in Figures 11-13.

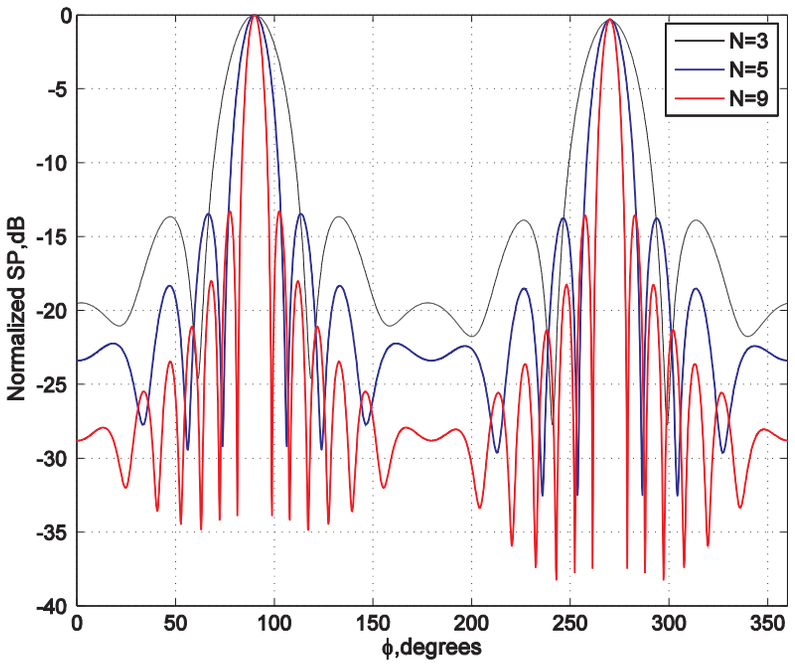

Figure 11. Scattering pattern of the 3-, 5- and 9-strip array φ_0=90 , $k=\pi$, t/w=0.1, d=1.5.

Figure 13 demonstrates the SP for the 3-, 5- and 9-element array with the same geometrical parameters, as in Figure 11, but for a different incidence angle, φ_0=30 , and wave number $k=kw$=2. With a small number of strips in the array, the shape of the main beam is not symmetric (the case N=3, Figure 12); for formation of a well-focused beam, it is necessary to increase the number of strips in the array. This assertion is confirmed by the substantially improved shape of the main scattering beam when element number increases to N=9.

http://dx.doi.org/10.5772/61287

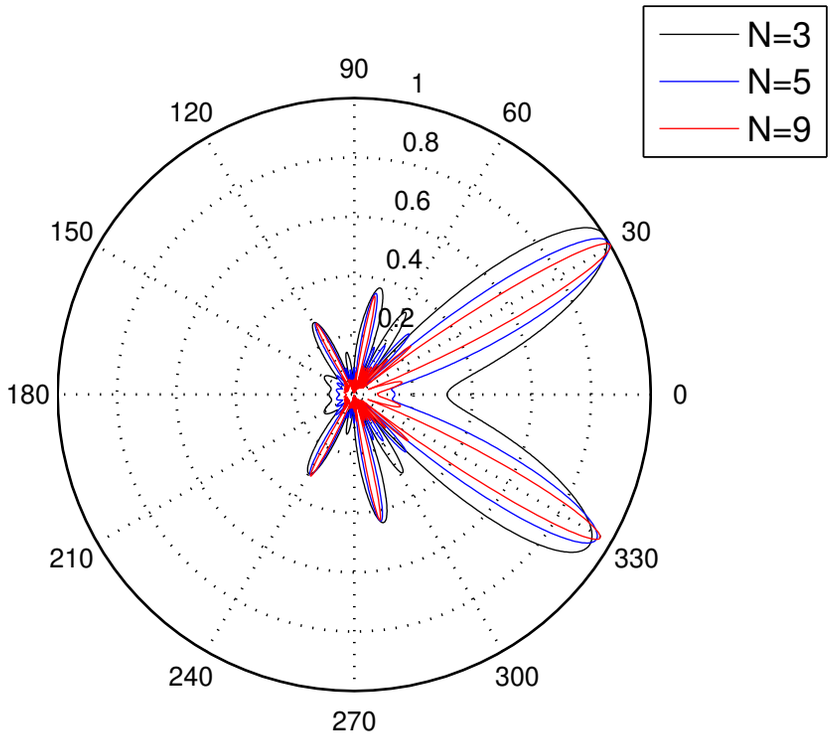

Figure 12. Scattering pattern of the 3-, 5- and 9-strip array ($\varphi_0=30$, $k=2\pi$, $t/w=0.1$, $d=1.5$).

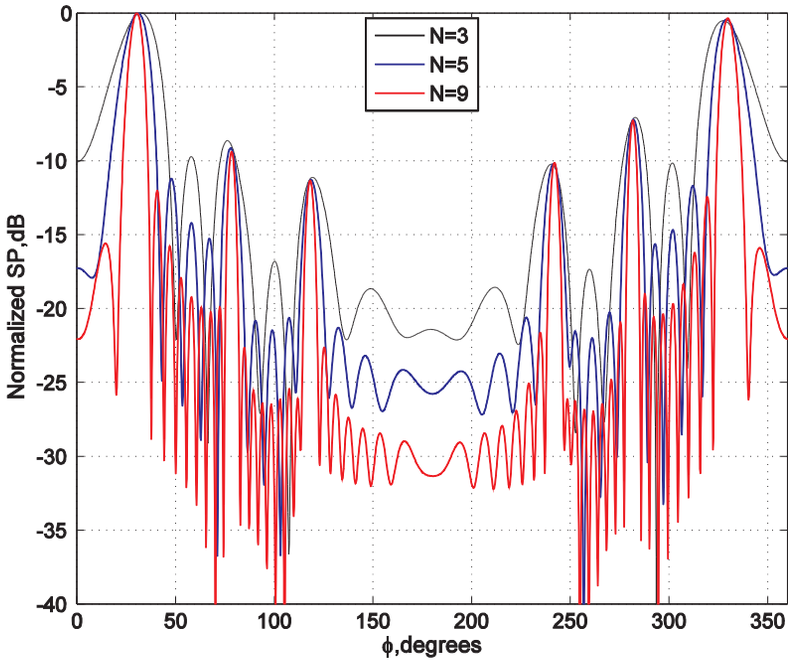

Figure 13. Scattering pattern in dB of the 3-, 5- and 9-strip array ($\varphi_0=30$, $k=2\pi$, $t/w=0.1$, $d=1.5$).

Next we consider the frequency dependence $RCS(k)$ of the RCS on wavenumber. Setting the array parameters: $N=3, 5, 9$ $w=1$, $t=0.1$, $d=1.5$, $\varphi_0=90$, we calculate the function $RCS(k)$ in the range $0 \le k \le 25$ (see Figure 14).

It is worth noting that extremely high values of the function $RCS(k)$ are explained by its normalization (the single element width was chosen to be a characteristic parameter, so that $k=kw$. For the 9-element array analysed above the total width W of the array is $W=9w+8(d-w)=13$ units (all sizes are related to the strip width); hence, $kW=13kw$. For comparison with the case of a single element case, the RCS should be scaled by the total width of array.

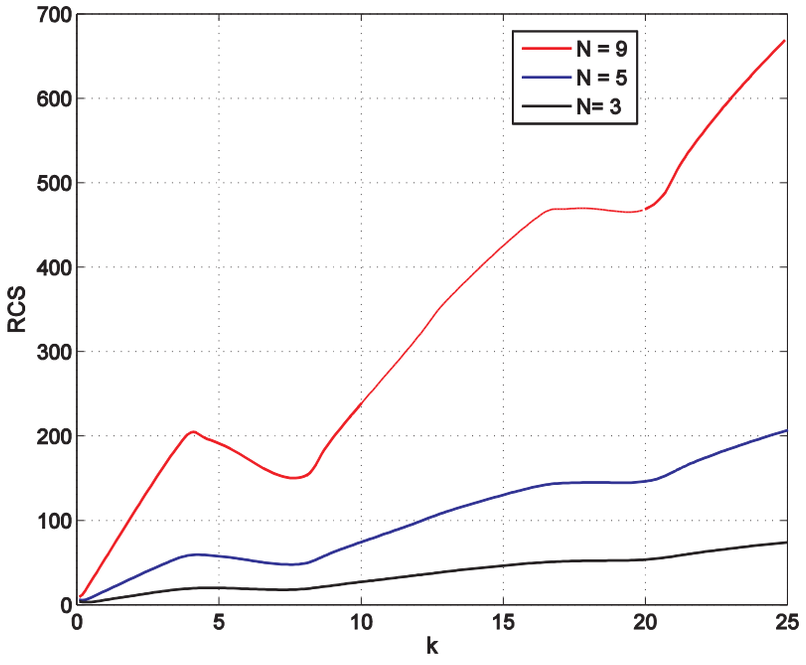

Figure 14. RCS versus relative wave number: $N=3, 5, 9; \varphi_0=90$, $t/w=0.1$, $d=1.5$.

The next graph in Figure 15 illustrates the effect of perturbing the periodicity of the array on the RCS: the central strip is moved towards to the neighbouring strip by a distance $d=0.4$. At the lower values of the relative wave number ($0 \le kw \le 1.8$), there is no influence of the non-symmetrical location of the central strip on the value of the RCS. At the value $kw=1.8$, the shift $g=0.9-0.5$ (see Figure 15) becomes slightly greater than the wave size $\lambda/9$. Hence, we can conclude that the disturbance in the location of the strip in the array is insignificant on the RCS when the shift does not exceed $\lambda/9$.

Now let us investigate how the thickness of the strips in an array impacts the RCS. In fact, we will consider a more general problem. Usually the term thick strip refers to the strip with the width w greater than its height h ($h/w<1$); otherwise, it is more reasonable to call such a

http://dx.doi.org/10.5772/61287

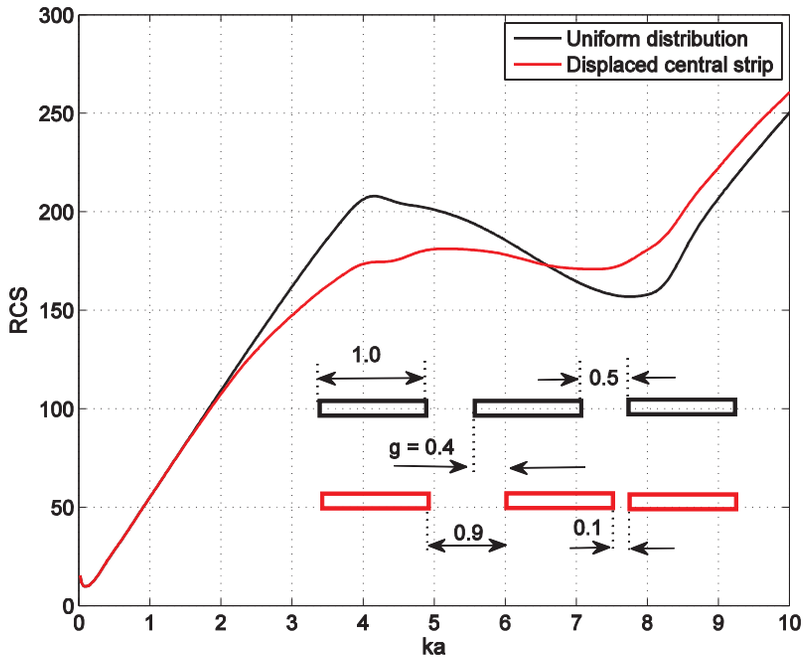

Figure 15. RCS of the 9-element periodic array (black) and array with shifted central strip (red): $N=9; \varphi_0=90$, $t/w=0.1$, $d=1.5$.

structure a rectangular or square bar ($h/w \geq 1$). The ratio $t=h/w=1$ represents a threshold value; the parameters w and h are better described as height and width as shown in Figure 16.

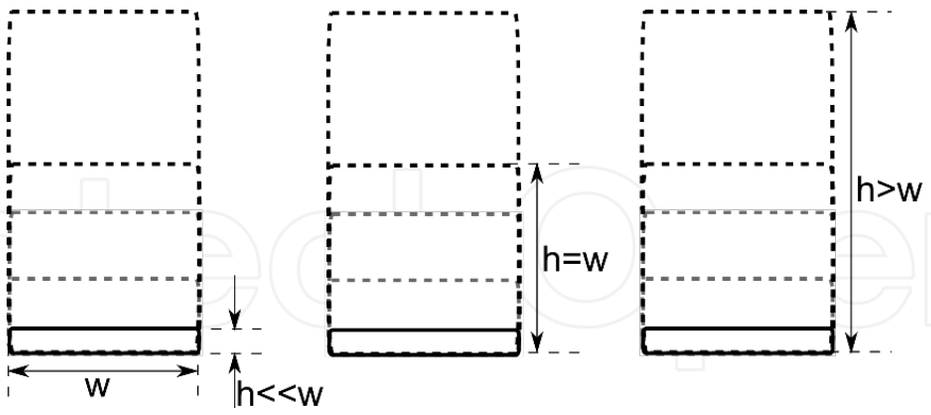

Figure 16. Schematic view of the strip thickening.

Here we consider normal wave incidence $\varphi_0=90$ on the array of strips with the fixed parameters: $w=1$, $d/w=3$, $k \equiv kw=\pi, 2\pi$ and 5π. Starting from the relative strip thickness $t=h/w=0.05$, we consider the dependence of RCS on t for a 3-element array in the range $0.05 \leq t=h/w \leq 3$. The results of these calculations are presented in Figure 17 ($k=\pi$), Figure 18 ($k=2\pi$) and Figure 19 ($k=5\pi$).

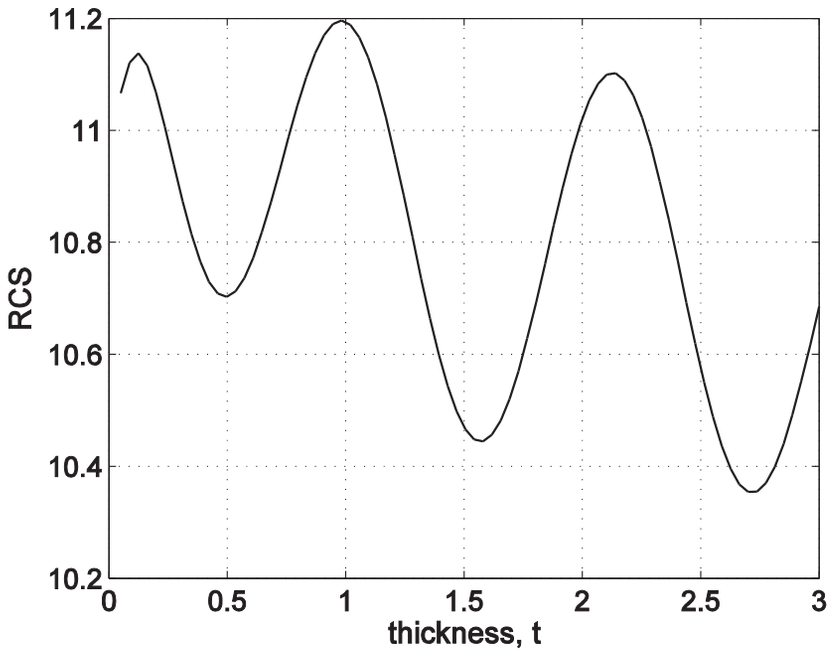

Figure 17. RCS of the 3-element array versus relative strip thickness t (φ_0=90 , $k=\pi$, $w=1$, $d=3$).

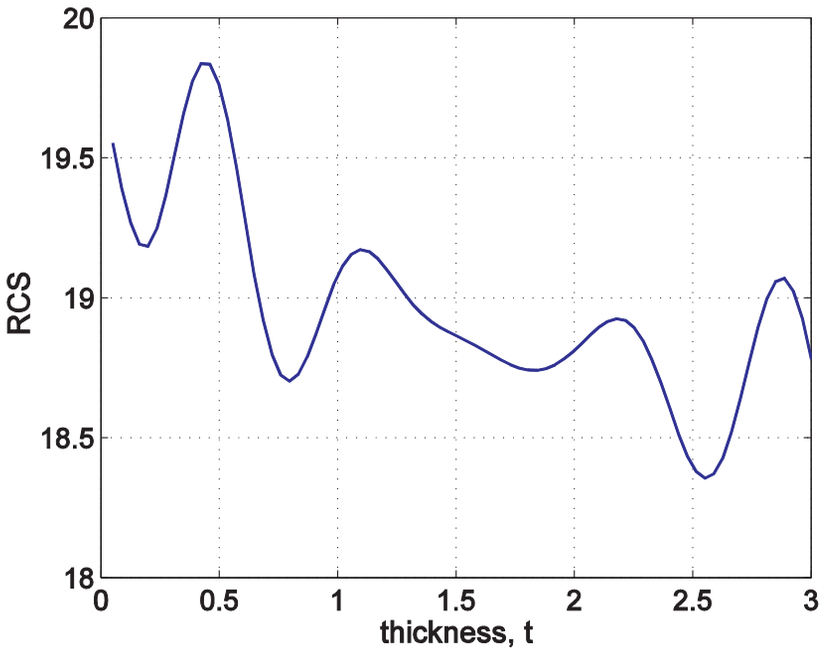

Figure 18. RCS of the 3-element array versus relative strip thickness t (φ_0=90 , $k=2\pi$, $w=1$, $d=3$).

http://dx.doi.org/10.5772/61287

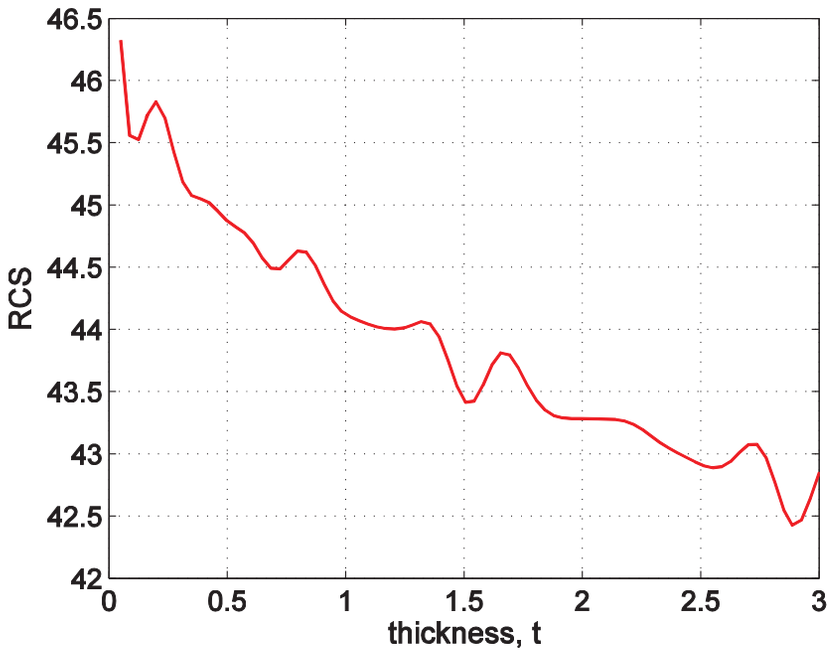

Figure 19. RCS of the 3-element array versus relative strip thickness t ($\varphi_0=90^\circ$, $k=5\pi$, $w=1$, $d=3$).

Surprisingly the RCS is fairly insensitive to substantial thickening of the original horizontal thin strip ($t=h/w=0.05$), even at the extreme transformation of the strip into a vertical rectangular cylinder with $t=h/w=3$. The difference between the maximum value $RCS(t)$ and its minimum value for the wavenumbers $k=\pi$ and $k=2\pi$ does not exceed 7.4%. In the case when $k=5\pi$, this difference increases to 8.3%.

4.2.2. Inclined arrays of thick strips

It was shown previously in this chapter that different positioning of the strips affects the reflection properties. Let us consider another geometry, arranging the strips as a 2D truncated corner reflector (see Figure 20).

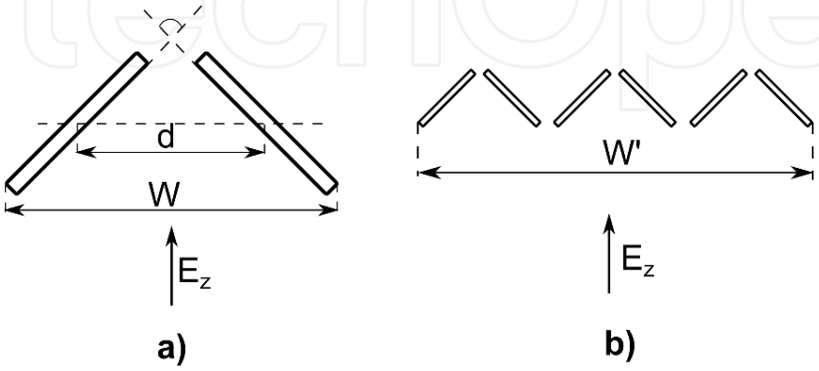

Figure 20. Truncated corner reflector ($\varphi_0=90^\circ$): (a) isolated reflector and (b) array of three reflectors.

Here we only consider normal wave incidence, so we normalize the function $RCS(k)$ by the characteristic maximum size of the structure. We define geometric parameters W for the single reflector and W' for the array of the corner reflectors (see Figure 20) by $W = d + (w + t)/\sqrt{2}$, $W' = 3W$, where d is the distance between strip centres, w and t are the single strip relative width and thickness, respectively. We calculate the dependence $RCS(kW)$ for the three values $d = 0.8, 1.2, 1.6$. As in previous calculations, we take $w = 1$, $t = 0.1$. The E-polarized plane wave excites the truncated corner reflector with incident angle $\varphi_0 = 90°$. The frequency dependence of the RCS in the range $0 < kW \leq 20$ for the single truncated corner reflector is shown in Figure 21.

The frequency dependence of the RCS in the range for the array of three truncated corner reflectors is shown in Figure 22. The RCS for the single truncated corner reflector is of a regular oscillatory character for each parameter $d = 0.8, 1.2, 1.6$; the average level of the RCS steadily grows along with the relative wave number. Combined as a 3-element array, a moderate enhancement of the RCS is observed. Closer spacing ($d = 0.8, 1.2$) of the reflectors preserves the regular oscillatory behaviour of the $RCS(kW)$, in contrast to more separated spacing ($d = 1.6$), where some peaks in the RCS graph (red, Figure 22) become suppressed.

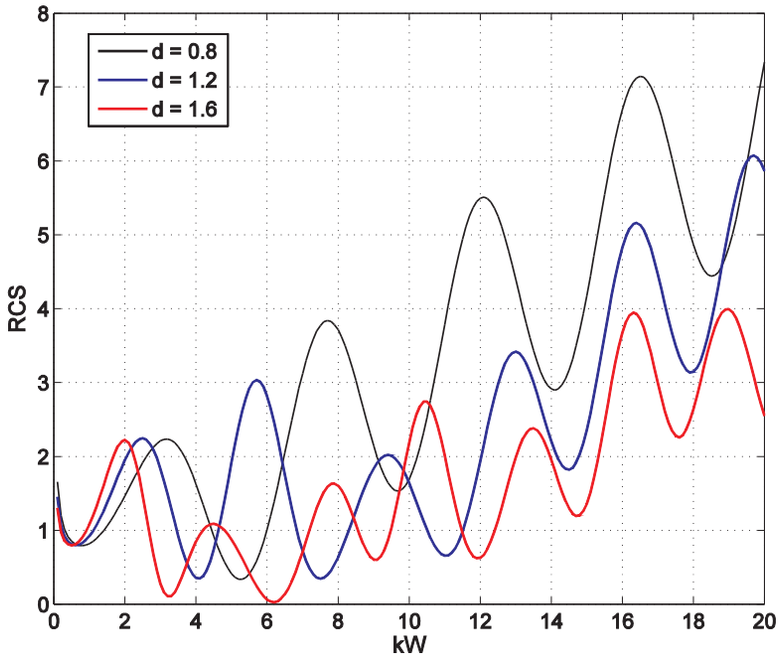

Figure 21. $RCS(kW)$ for the single corner reflector: $\varphi_0 = 90$, $w = 1$, $t = 0.1$.

http://dx.doi.org/10.5772/61287

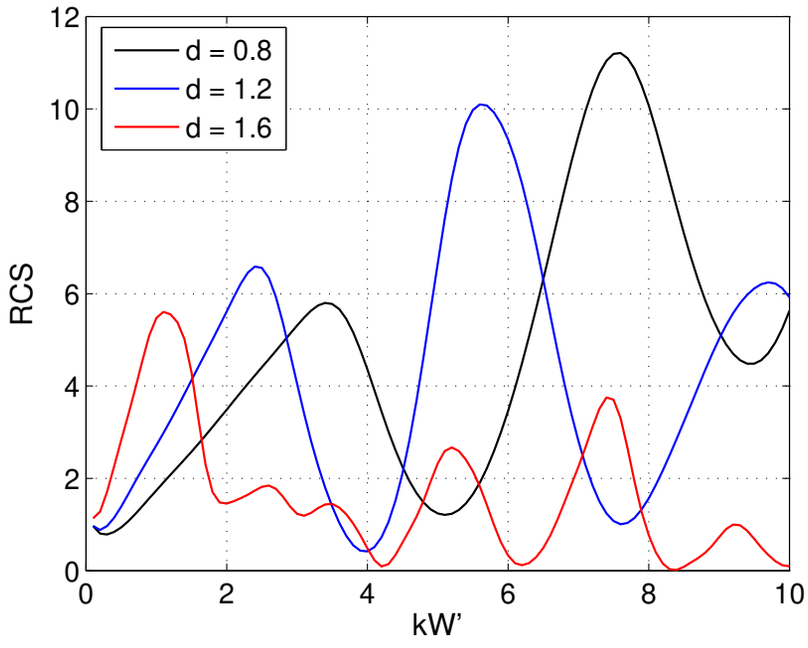

Figure 22. $RCS(kW')$ for the array of three corner reflectors: $\varphi_0=90$, $w=1$, $t=0.1$.

5. Conclusion

In this chapter, a rigorous approach to the numerical analysis of the multi-conductor problems in electrostatics and multiple wave scattering for metallic cylinders is presented. The problems are treated as a classical Dirichlet boundary value problem for the Laplace and Helmholtz equations. All conductors may be of arbitrary cross-sections; the only restriction on the system geometry is a smooth parameterization of the boundaries.

The 2D multi-conductor problems for the Laplace and Helmholtz equations are rigorously solved by the MAR. The problem is transformed to a numerical analysis of an infinite system of linear algebraic equations of the second kind. This explains its fast convergence and guaranteed computational accuracy, depending only upon truncation number N_{tr}. The computation of the matrix elements is based on the discrete FFT, making the matrix filling an accurate and extremely fast procedure. The only limitation imposed on the contour is its smoothness. When the contour incorporates corners, they should be rounded. The developed algorithm is numerically stable and fast, and accuracy of the solution can be pre-specified. The solution obtained is applied to the accurate analysis of 2D electrostatic and electrodynamic field problems for multi-conductor systems with arbitrary profiled conductors. Examples for some conceptual shielded transmission lines incorporating differently profiled conductors and scattering problems for the arrays of thick strips illustrate the efficiency and reliability of the method.

Author details

Galyna Safonova* and Elena Vinogradova

*Address all correspondence to: galyna.saf@gmail.com

Department of Mathematics, Macquarie University, Sydney, Australia

References

[1] Jackson JD. *Classical Electrodynamics*. New York: Wiley; 1999. p. 808.

[2] Shi F, Ramesh P and Mukherjee S. On the Application of 2D Potential Theory to Electrostatic Simulation. *Communications in Numerical Methods in Engineering* 1995; 11(8): 691-701.

[3] Paul CR. *Analysis of Multiconductor Transmission Lines*. New York: Wiley; 1994.

[4] Brando Faria JA. Multiconductor Transmission Lines. *Encyclopedia of RF and Microwave Engineering*; 2005.

[5] Kamchouchi HE and Zaky AA. A Direct Method for the Calculation of the Edge Capacitance of Thick Electrodes. *Journal of Physics D* 1975; 8: 1365-1371.

[6] Moreira FJS and Prata A. Vector-Diffraction Analysis of Finite Perfectly Conducting Gratings with Arbitrary Profiles. *Journal of Microwaves and Optoelectronics* 1999; 1(5): 11-13.

[7] Filtz M and Henke H. Planar Millimeter Wave Structures. *Electrical Engineering (Archiv fur Elektrotechnik)* 2004; 86(2): 147-155.

[8] Mata-Mendez O, Avendao J and Chavez-Rivas F. Rigorous Theory of the Diffraction of Gaussian Beams by Finite Gratings: TM Polarization. *Journal of Optical Society of America A* 2006; 23(8): 1889-1896.

[9] Borghi R, Gori F and Santarsiero M. Plane-Wave Scattering by a Set of Perfectly Conducting Circular Cylinders in the Presence of a Plane Surface. *Journal of Optical Society of America A* 1996; 13(12): 2441-2452.

[10] Argatov II and Sabina FJ. Acoustic Scattering by a Cluster of Small Sound-Soft Obstacles. *Wave Motion* 2010; 47(8): 537-551.

[11] Yang J, Li LW, Yasumoto K and Liang CH. Two-Dimensional Scattering of a Gaussian Beam by a Periodic Array of Circular Cylinders. *IEEE Transactions on Geoscience and Remote Sensing* 2005; 43(2): 280-285.

[12] Yasumoto K, Toyama H and Kushta T. Accurate Analysis of Two-Dimensional Electromagnetic Scattering from Multilayered Periodic Arrays of Circular Cylinders Us-

ing Lattice Sums Technique. *IEEE Transactions on Antennas and Propagation* 2004; 52(10): 2603-2611.

[13] Lucido M, Panariello G and Schettino F. Electromagnetic Scattering by Multiple Perfectly Conducting Arbitrary Polygon Cylinders. *IEEE Transactions on Antennas and Propagation* 2008; 56(2): 425-436.

[14] Judd SV, Whiteley I, Clowes RJ and Rickard DC. An Analytical Method for Calculating Microstrip Transmission Line Parameters. *IEEE Transactions on Microwave Theory and Techniques* 1970; 18(2): 78-87.

[15] Zhu NH, Qiu W, Pun EYB and Chung PS. Quasi-Static Analysis of Shielded Microstrip Transmission Lines with Thick Electrodes. *IEEE Transactions on Microwave Theory and Techniques* 1997; 45(2): 288-290.

[16] Chang T and Tan C. Analysis of a Shielded Microstrip Line with Finite Metallization Thickness by the Boundary Element Method. *IEEE Transactions on Microwave Theory and Techniques* 1990; 38(8): 1130-1132.

[17] Gentili GG and Macchiarella G. Quasi-Static Analysis of Shielded Planar Transmission Lines with Finite Metallization Thickness by a Mixed Spectral-Space Domain Method. *IEEE Transactions on Microwave Theory and Techniques* 1994; 42(2): 249-255.

[18] Khebir A, Kouki AB and Mittra RM. Higher Order Asymptotic Boundary Condition for Finite Element Modeling of Two-Dimensional Transmission Line Structures. *IEEE Transactions on Microwave Theory and Techniques* 1990; 38(10): 1433-1438.

[19] Slade GW and Webb KJ. Computation of Characteristic Impedance for Multiple Microstrip Transmission Lines Using a Vector Finite Element Method. *IEEE Transactions on Microwave Theory and Techniques* 1992; 40(1): 34-40.

[20] Alam MS, Hirayama K, Hayashi Y and Koshiba M. Analysis of Shielded Microstrip Lines with Arbitrary Metallization Cross Section Using a Vector Finite Element Method. *IEEE Transactions on Microwave Theory and Techniques* 1994; 42(11): 2112-2117.

[21] Yee HY and Wu K. Printed Circuit Transmission-Line Characteristic Impedance by Transverse Modal Analysis, *IEEE Transactions on Microwave Theory and Techniques* 1986; 34(11): 1157-1163.

[22] Hong IP, Yoon N, Park SK and Park HK. Investigation of Metal-Penetrating Depth in Shielded Microstrip Line. *Microwave and Optical Technology Letters* 1988; 19(6): 396-398.

[23] Zaki KA and Neureuther AR. Scattering from a Perfectly Conducting Surface with a Sinusoidal Height Profile: TM Polarization. *IEEE Transactions on Antennas and Propagation*1971; 19(6): 747-751.

[24] Booker SM and Vinogradov SS. A Two Body Benchmark Problem for Transient and Ultrawideband Scattering. *Journal of Electromagnetic Waves and Applications* 2002; 16(3): 365-384.

[25] Nosich AI. The Method of Analytical Regularization in Wave-Scattering and Eigenvalue Problems: Foundations and Review of Solutions. *IEEE Transactions on Antennas and Propagation* 1999; 41(3): 34-48.

[26] Smith PD. Recent Advances in Regularization Techniques for Scattering and Diffraction. *Radio Science* 2007; 42(6): doi: 10.1029/2007RS003703.

[27] Kellogg O. *Foundations of Potential Theory*. Berlin-Heidelberg-New York: Springer-Verlag; 1967.

[28] Colton D and Kress R. *Integral Equation Methods in Scattering Theory*. New York: John Wiley & Sons; 1983.

[29] Kress R. *Linear Integral Equations, ser. Applied Mathematical Sciences*. Berlin: Springer-Verlag (Volume 82); 1989.

[30] Vinogradov SS, Smith PD and Vinogradova ED. *Canonical Problems in Scattering and Potential Theory, Part 1: Canonical Structures in Potential Theory*. Boca Raton: Chapman & Hall/CRC; 2001.

[31] Vinogradov SS, Vinogradova ED, Wilson C, Sharp I and Tuchkin YA. Scattering of an E-Polarized Plane Wave by Two-Dimensional Airfoils. *Electromagnetics* 2009; 29(3): 268-282.

[32] Vinogradova ED and Smith PD. *Diffraction from 2-D Arbitrary Structures with Cavities or Edges: A Rigorous Approach: Proceedings of the XXVIIth General Assembly of URSI*, URSI GASS, 2002, The Netherlands, Maastricht.

[33] Shestopalov VP, Tuchkin YA, Poedinchuk AE and Sirenko YK. *New Methods of Solving Direct and Inverse Problems of Diffraction Theory*. Kharkiv: Osnova (In Russian); 1997.

[34] Kantorovich LV and Akilov GP. *Functional Analysis in Normed Spaces*. New York: Pergamon Press; 1974.

[35] Collin RE. *Field Theory of Guided Waves*. Oxford: Oxford University Press; 1991.

[36] Yakover YM. General Analysis of Shielded Transmission Lines with Cylindrical Geometry Conductors. *27th European Microwave Conference* 1997; 2: 955-958.

[37] Malits P, Haridim M and Chattah Y. Characteristic Impedance of a Shielded Transmission Line with Non-Concentric Arc-Shaped Conductors. *Electromagnetics* 2009; 29: 337-352.

[38] Jielis J. A Generic Geometric Transformation That Unifies a Wide Range of Natural and Abstract Shapes. *American Journal of Botany* 2003; 90(3): 333-338.

[39] Safonova G, Vinogradova ED and Tuchkin Y. Accurate Impedance Calculations for Transmission Lines with Adjustable Inner Conductor. *Microwave and Optical Technology Letters* 2014; 56(9): 2066-2070.

[40] Safonova G and Vinogradova ED. Rigorous Approach to Calculation of Capacitance Images of Metallic Samples for Use in Capacitance Microscopy. *Progress in Electromagnetics Research B* 2013; 55: 383-399.

[41] Honey R. A Flush-Mounted Leaky-Wave Antenna with Predictable Patterns. *IEEE Transactions on Antennas and Propagation* 1959; 7(4): 320-329.

[42] Klohn KL, Horn RE, Jacobs H and Freibergs E. Silicon Waveguide Frequency Scanning Linear Array Antenna. *IEEE Transactions on Microwave Theory and Techniques* 1978; 26(10): 764-773.

[43] Brand GF. The Strip Grating as a Circular Polarizer. *American Journal of Physics* 2003; 71(5): 452.

[44] Kobayashi K and Miura K. Diffraction of a Plane Wave by a Thick Strip Grating. *IEEE Transactions on Antennas and Propagation* 1989; 37(4): 459-470.

[45] Peng ST and Shiao CM. Scattering of Plane Waves by Metallic Gratings. Microwave Symposium Digest. *IEEE MTT-S International* 23-27 May 1994; 2: 879-882, doi: 10.1109/MWSYM.1994.335217.

[46] Filipovic D and Dlabac T. Low Frequency TM Plane-Wave Scattering from a Two-layer Double-strip Grating with Equal Gaps. *Series: Electrical Energy* 2006; 19(3): http://www.doiserbia.nb.rs/img/doi/0353-3670/2006/0353-36700603379F.pdf (accessed 9 September 2014).

[47] Shimoda M and Itakura T. Scattering of Electromagnetic Plane Waves by an Inclined Parallel Strip Grating. *Electronics and Communications in Japan (Part II: Electronics)* 1990; 73(8): 56-65.

[48] Safonova G and Vinogradova ED. Accurate Backscattering Studies for Double-Layered Array of Infinitely Long Cylinders. *Microwave and Optical Technology Letters* 2013; 55: 2127-2131.

[49] Kalhor HA. Plane Metallic Gratings of Finite Number of Strips. *IEEE Transactions on Antennas and Propagation* 1989; 37(3): 406-407.

IntechOpen